Characterization of Combined Longitudinal and Transverse FRPs for Strengthening Concrete Columns

Pedram Sadeghian[1] and Brandon Fillmore

Department of Civil and Resource Engineering, Dalhousie University, Halifax, NS, B3H 4R2, Canada.

ABSTRACT: This paper presents the results of a study on the characterization of combined longitudinal near-surface-mounted (NSM) fiber-reinforced polymer (FRP) bars and transverse FRP wraps for strengthening concrete columns. A total of 21 concrete cylinders were prepared, strengthened, and tested to characterize the performance of the strengthening system. Three arrangements of glass FRP (GFRP) bars were mounted in surface grooves, and unidirectional basalt FRP (BFRP) composite was used to wrap the specimens. It was shown that the wrapping system effectively prevented the premature failures of the NSM bars and extended the contribution of the bars from an average of 17.5% in the NSM specimens to an average of 27.7% in the specimens strengthened with the combined NSM and transverse FRPs. An analytical model was also presented to predict the load-strain behavior and the effect of combined axial load and bending moment.

KEYWORDS: FRP, strengthening, column, buckling, crushing, rupture.

DOI: http://dx.doi.org/10.1139/cjce-2018-0813

[1] Corresponding Author: Pedram.Sadeghian@dal.ca

1. INTRODUCTION

Strengthening concrete beams and slabs using near-surface mounted (NSM) fiber-reinforced polymer (FRP) bars and strips has gained significant research interest due to the effectiveness of NSM technique in preventing/delaying debonding of NSM FRP from concrete (De Lorenzis and Nanni 2001; Hassan and Rizkalla 2003; Hosseini et al. 2014). However, the method has not been effectively implemented for concrete columns due to the possibility of buckling of NSM bars/strips. On the other hand, FRP wrapping has been successfully used to enhance the axial capacity of concrete columns with limited effect on bending performance at low level of axial load (Rocca et al. 2009; Bisby and Ranger 2010; Sadeghian and Fam 2014). As most columns are subjected to both combined axial load and bending moment, it is crucial for practicing engineers to enhance both axial and bending capacities. The longitudinal NSM bars can provide flexural strength and the transverse FRP wraps provide lateral support for the NSM bars and confinement for the concrete core. The FRP wrap can also provide additional shear strength and protects the concrete core and existing steel bars against harsh environments. The combination of longitudinal NSM FRPs and transverse FRP wrapping (hereafter is called NSM-wrap system) can provide a durable and cost-effective solution for strengthening of bridge columns/piers and waterfront structures with concrete piles/columns.

NSM systems are defined by ACI 440.2R-17 (2017) as circular or rectangular bars or plates installed and bonded into grooves made on the concrete surface. Two common FRP bar types have been used for NSM applications, namely round bars and rectangular bars/plates/strips. They are usually manufactured using pultrusion processes and typically delivered to the site in the form of either single bar or a roll. A suitable adhesive should be used to bond the NSM FRP into the groove to be cured in-place. The adhesive provides a shear transfer between the concrete substrate and the

NSM FRP. It should be noted that ACI 440.2R-17 considers FRPs only in tension and ignores any contribution of FRP bars/strips in concrete under direct compression. Per ACI 440.2R-17, while FRP materials can support compressive stresses, there are numerous issues surrounding the use of FRP for compression. Micro buckling of fibers can occur if any resin voids are present in the laminate. Laminates themselves can buckle if not properly adhered or anchored to the substrate, and highly unreliable compressive strengths result from misaligning fibers in the field. It is acceptable, however, for FRP tension reinforcement to experience compression due to moment reversals or changes in load pattern. The compressive strength of the FRP reinforcement, however, should be neglected. ACI 440.1R-15 (2015) also neglects the compressive contribution of internal FRP bars based on the same approach.

There are numerous experimental studies indicating that internal FRP bars can support a significant level of compressive strain if sufficient lateral support is provided. Tobbi et al. (2012) tested large-scale columns and concluded that glass FRP (GFRP) bars could be used in compression members if adequate transverse bars are provided to eliminate bar buckling. Recently, Karim et al. (2016) found that longitudinal GFRP bars improved the peak load and the ductility of the columns. Also, Hadhood et al. (2017) reviewed and discussed the compressive contribution of GFRP bars and found that ignoring the contribution of the compression GFRP bars underestimated the nominal axial load and moment capacity of the tested columns. More recently, Fillmore and Sadeghian (2018) found that the elastic modulus of GFRP bars in compression is slightly higher than that in tension; however, the compressive strength was obtained at 67% of tensile strength. Moreover, Khorramian and Sadeghian (2017) showed that GFRP bars can be considered as load bearing longitudinal reinforcement of concrete columns and ignoring their effect is not necessary.

The behavior of the NSM-wrap system for strengthening concrete columns was initially studied by Bournas and Triantafillou (2009) and El-Maaddawy and El-Dieb (2010) in late 2000's. In addition, there is a report on the application of the system in the form of FRP bar and FRP sheet for strengthening a residential concrete column in Calgary, Alberta, Canada in 1999. However, the system has not been adopted by design guides and codes due to limited studies on the behavior of the system and concerns regarding the behavior of longitudinal FRPs in compression as mentioned earlier. Bournas and Triantafillou (2009) demonstrated that NSM FRP reinforcement is a viable solution toward enhancing the flexural resistance of concrete columns subjected to seismic loads. This was especially the case when the retrofitting scheme combines epoxy-bonded NSM bars with local confining jackets with textile-reinforced mortars (TRM). Moreover, El-Maaddawy and El-Dieb (2010) found that the effectiveness of the NSM GFRP reinforcement was greatly affected by the FRP confinement level and the load eccentricity. Based on the literature, it is concluded that NSM FRPs are also effective for concrete columns under significant bending, and their effectiveness increases by applying FRP wraps. However, due to limited data, the behavior of the NSM-wrapped system with the approach of extending the contribution of NSM FRPs beyond the typical strain level of concrete in compression has not been studied. In addition, basalt fibers have been recently emerged to the market with environmental and economical advantages (Fiore et al. 2015) over traditional glass fibers. Basalt FRP (BFRP) composites can be a viable replacement of externally bonded GFRP sheets for strengthening existing concrete structures.

The use of longitudinal NSM FRP bars for strengthening existing concrete columns has not gained much attention due to the possibility of premature crushing and/or buckling of NSM bars. The focus of this study is to test the NSM-wrap system combining both NSM and wrapping methods to prevent the premature failure and extend the contribution of NSM bars through

extended strain of confined concrete. The results can open a new avenue in the strengthening of existing concrete columns where the combination of longitudinal and transverse reinforcements is needed to upgrade both axial and flexural capacities. The NSM-wrap strengthening system can be also effective for bridge columns under lateral wind or seismic loadings.

In this study, a total of 21 plain concrete cylinders were prepared, strengthened, and tested to characterize the performance of the NSM-wrap system of longitudinal NSM GFRP bars and transverse BFRP wraps. Multiple GFRP bars were mounted into surface grooves and unidirectional BFRP was used to wrap the specimens. Test parameters were the number of NSM GFRP bars (4, 6, and 8) and number of BFRP layers (0 and 2). Plain specimens were also tested as control specimens. The specimens were instrumented with multiple strain and displacement gauges and loaded under uniaxial compression up to failure. An analytical model is also presented to predict the load-strain behavior of the test specimens. In addition, to predict the effectiveness of the system for other loading condition and provide a direction for future studies, an analytical model was implemented and verified against independent test data to perform a parametric study on the effect of load eccentricity on the interaction axial load – bending moment diagram of concrete columns strengthened using the NSM-wrap system.

2. EXPERIMENTAL PROGRAM

This section presents the details of test matrix, material properties, specimen preparation, test setup, and instrumentation of the test specimens.

2.1. Test Matrix

A total of 21 concrete cylinders with a diameter of 150 mm and a height of 300 mm were prepared and tested under uniaxial compression loading. The testing matrix consisted of control groups of

plain and GFRP NSM-reinforced concrete specimens (i.e. NSM-4, NSM-6, and NSM-8), and GFRP NSM-reinforced concrete specimens wrapped with two layers of BFRP (i.e. NSM-4-W, NSM-6-W, and NSM-8-W). As shown in Figure 1, the NSM bars were placed in 4, 6, and 8 bar arrangements with nominal diameters of 13 mm (#4). Table 1 shows the test matrix. Three identical specimens per group were prepared and tested.

2.2. Material Properties

Ready mix concrete with maximum aggregate size of 13 mm and slump of 100 mm was delivered. The average compressive strength of concrete at the time of test was 40 MPa. Round GFRP bars with nominal diameter of 13 mm (#4) and nominal cross-sectional area of 126.7 mm^2 were used as NSM bars. A guaranteed tensile strength, elastic modulus, and rupture strain of 758 MPa, 46 GPa, and 1.64%, respectively, per the manufacturer (Aslan FRP 2018). It should be noted that the GFRP bars used in this study were available at Dalhousie University from an old batch at the time of the research and were not the latest product of the manufacturer. An adhesive was used as the bonding material to secure the NSM bars into the groove of the concrete specimens. The tensile strength, tensile elastic modulus, ultimate tensile strain, and the bond strength of the adhesive were 27.6 MPa, 3.06 GPa, 1.0%, and 13.8 MPa, respectively, as reported by the manufacturer (BASF 2014).

Three GFRP bar coupons were prepared and tested in tension per ASTM D7205 (2006). Two strain gauges were attached on the surface of the bars at the mid-length of the specimen. The average of two strain gauges was used to plots stress-strain curves as shown in Figure 2(a). The average ± standard deviation of the tensile strength, tensile elastic modulus, and tensile rupture strain of GFRP bars were obtained as 839±49 MPa, 44.2±1.7 GPa, and 0.0209±0.0021 mm/mm, respectively. As there is no standard method for testing FRP bars in compression, a new test

method proposed by Khorramian and Sadeghian (2009) was implemented through applying pure compression load on five short GFRP bar specimens with a free length twice the diameter of the bars. Figure 2(b) shows the test setup. Two strain gauges were attached on the surface of the bars at mid-length. Mode of failure of rebars in compression test was crushing and no global buckling was observed during the test.

It should be highlighted that the test was designed to prevent global buckling of the bars using the length/diameter ratio of 2. The average ± standard deviation of compressive strength, elastic modulus, and ultimate strain of GFRP were obtained as 559±36 MPa, 45.5±1.5 GPa, and 0.0122±0.0012 mm/mm, respectively. Figure 2 shows the stress-strain diagram obtained from the compression tests. Both tension and compression loads were applied with a rate of 2 mm/min. The tensile and compressive elastic modulus was calculated based on a chord modulus ranging from a strain of 0.001 to 0.003 mm/mm. It was observed that the compressive strength of GFRP bars in compression was 67% of tensile strength. Also, the elastic modulus of GFRP rebar tested in compression was slightly higher than that of in tension, which justify the assumption of having the same elastic modulus in tension and compression. It means ignoring compressive strength of GFRP bars and considering their strength and modulus like concrete in compression is not realistic. It should be noted that the performance of GFRP bars in concrete could be different than coupon test.

For wrapping, a unidirectional basalt fabric and epoxy resin were used. For resin, a mixture of epoxy resin and slow hardener was used, which was reported by the manufacturer (West System 2015) to have the tensile strength, tensile modulus, and maximum elongation of 50 MPa, 2.8 GPa, and 4.5%, respectively. The epoxy resin was reinforced by a unidirectional basalt fabric with the areal weight of 300 g/m^2 and nominal thickness of 0.115 mm. The tensile strength, tensile modulus,

and rupture strain of basalt fibers were 2100 MPa, 105 GPa, and 2.6%, per the manufacturer (Unistar 2016). Five identical BFRP tensile coupons made of two layers of the unidirectional fabric and epoxy resin were prepared using wet hand lay-up method and tested according to ASTM D3039 (2008) with a displacement rate of 2 mm/min was used. A strain gauge was applied on each side of the coupons, centered in the longitudinal direction of fibers/coupon to measure the axial strain. Figure 2 shows the tensile test results of five identical coupons based on the average ply thicknesses of 0.45 mm. The tensile strength and elastic modulus of BFRP coupons were obtained 624.1±17.2 MPa and 24.62±0.08 GPa, respectively (average ± standard deviation). It should be highlighted that strain gauges were stopped reading strain in a range between 0.0156 and 0.0167 mm/mm due to either internal malfunction or reaching to their calibration limit. As the coupons were made of unidirectional fabric, the stress-strain curves were extended with the same modulus to the average tensile strength, which was resulted in the extrapolated rupture strain of 0.0253 mm/mm. This is compatible with the manufacturer rupture strain of 0.026 mm/mm for basalt fibers as shown in Figure 2(a).

2.3. Specimen Preparation

Standard plastic molds with the inner diameter of 150 mm and height of 300 mm were used for the fabrication of concrete specimens. Due to the high risk of working with a concrete saw, it was decided to install 300-mm long wooden sticks with 25 mm x 25 mm cross-section to the inner surface of the plastic molds with a radial arrangement accommodating 4, 6, or 8 NSM grooves. Figure 3 shows the procedure. The fresh concrete was placed and consolidated in two layers using scoops, a vibration table, and then the surface was carefully troweled smooth. The consolidated concrete was left in the molds and covered to moist cure for 4 days before the molds were removed and the specimens were relocated to the laboratory. After at least 28-days, the wooden sticks were

removed and the specimens were left in the lab to cure and dry. Then the grooves were cleaned with a wire brush for the strengthening procedure.

As shown in Figure 4, the grooves were partially filled with the adhesive, the NSM bar was placed into the center of the groove, and then the groove was filled with adhesive. A blade was used to make the surface of the groove flat and compatible with the curvature of the concrete cylinder. After at least a 7-day curing, two layers of the unidirectional basalt fabric was continuously applied in the hoop direction using the epoxy resin. An overlap of 100 mm was applied to the last layer of the wrap. Also, a 40-mm strap made of two layers of the basalt fabric was applied at each end of all cylinders to ensure the ends are strong enough to prevent localized end failure. The specimens then were capped with a Sulphur compound for uniform loading.

2.4. Test Setup and Instrumentation

As shown in Figure 5, the axial deformation of the specimens was measured using two linear variable differential transformer (LVDT) units fixed to the cylinder using aluminum brackets over 150 mm gauge lengths. Two NSM bars per specimens were also instrumented with 12 mm longitudinal strain gauges each, which were bonded to flat surfaces machined in-house into the outward facing sides of the bars. For each wrapped specimen, four more strain gauges were installed on the BFRP wrap, two in the axial direction and two in the hoop direction at locations 90 degrees apart as shown in Figure 5. For unwrapped specimens, two horizontal LVDTs were also placed at mid-height of each specimen in a radial direction at locations 180 degrees apart. The compressive testing was done on a 2 MN universal testing machine and was programmed to deform the specimens at a rate of 0.6 mm per minute. The specimens were compressed until the BFRP wrap was ruptured. During the tests, the axial load, stroke, displacement of LVDTs, and

strain of strain gauges were collected at a rate of 10 data point per second using a digital data acquisition system.

3. TEST RESULTS AND DISCUSSION

Table 2 shows the summary of the test results. The average (AVG) and standard deviation (SD) of the peak load, axial and lateral strains at peak load, NSM bars force at peak load, and NSM bars contribution at peak load of each group of specimens are presented in the Table. In this section, the results are discussed in detail along the failure mode, load-strain behavior of the specimens, and NSM bars contribution.

3.1. Failure Mode

Figure 6 shows some of the specimens after the test. The control group of plain concrete specimens all failed along a shear plane, and some light tapping with a hammer revealed that fractures were developed all around the upper and lower shear cones. NSM specimens' failure was controlled by concrete crushing. As concrete passed its crushing strain and started to bulge significantly, NSM bars buckled and some of them crushed, as shown in Figure 6(a). Overall, NSM bars did not show any signs of crushing until the concrete bulged and cracked significantly. As shown in Figure 6(b), the behavior of NSM-wrapped specimens was completely different than NSM specimens without wrapping. NSM bars were continued contributing to the load bearing system and did not buckle until the FRP wrap was ruptured in the hoop direction, long after the other specimens. In some specimens, before the FRP wrap rupture, the NSM bars started to crush making noise and dropping the load. FRP wraps were typically ruptured at the location of the NSM bars, indicating lateral concentrated pressure on the FRP wrap can control the rupture. Overall, FRP wraps were effective on extending the contribution of the NSM bars.

3.2. Load-Strain Behavior of NSM Specimens

Figure 7 shows the axial load vs. axial and lateral strain curves of three identical specimens of each group of control plain and NSM specimens. As shown, all NSM and plain specimens followed almost the same path until an axial load of about 700 kN and axial strain of about 0.0028 mm/mm, where the plain specimens lost significant stiffness. As presented in Table 2, the plain specimens peaked to an average axial load of 707 kN and corresponding average axial and lateral strains of 0.0030 and 0.0020 mm/mm, respectively, and then followed to a softening branch until the concrete was completely crushed or the test was terminated for safety reason. As shown in Figure 7, the NSM specimens continued gaining load and after a peak load slightly larger than plain specimens they started their softening branch. Based on the data presented in Table 2, the specimens with 4, 6, and 8 NSM bars peaked at higher axial loads with the average gain of 3.0, 2.1, and 8.1% with respect to the plain specimens, respectively. The specimens with 6 NSM bars showed a gain less than those with 4 NSM bars, which can be due to the variability of test results for both NSM-4 and -6 with 22 and 21 kN standard deviation, respectively.

The important effect of NSM bars was increasing the axial deformability of the specimens. Based on the data presented in Table 2, the axial strain of the specimens with 4, 6, and 8 NSM bars at peak load showed the average gain of 13.8, 12.5, and 23.9%, respectively, with respect to that of the plain specimens. Moreover, the lateral strain of the specimens with 4, 6, and 8 NSM bars at peak load showed the average gain of 62.0, 93.8, and 74.6%, respectively, with respect to that of the plain specimens. It means the effect of NSM bars was more pronounced on the lateral deformability of the specimens as it can be seen in Figure 7. In addition, the softening branch of the NSM specimens had more gradual softening in comparison with that of the plain specimens. Overall, the peak load and the axial and lateral strains corresponding to the peak load increased as

the amount of NSM reinforcement increased. In addition, the lateral strain at peak load was affected more than the peak load itself. The average axial and lateral strains at peak load of NSM specimens was 0.0035 and 0.0036 mm/mm, which are larger than those of the plain specimens, i.e. 0.0030 and 0.0020 mm/mm, respectively.

It should be noted that, the NSM-wrapped specimens, experienced gradual capping crushing at the ends, possibly due to stress concentration at the location of the NSM bars. The gradual capping crushing caused small noise in the load-strain curves as shown in Figure 8. Large drops were typically due to crushing of NSM bars. For the future tests, it is recommended to make NSM bars slightly shorter than the height of the test specimen to minimize the noise.

3.3. Load-Strain Behavior of NSM-Wrapped Specimens

Figure 8 shows the axial load vs. axial and lateral strain curves of three identical specimens of each group of NSM and NSM-wrapped specimens. As shown, FRP wrap changed the behavior of the NSM specimens significantly, increasing both peak load and its corresponding strain. There is clearly an interaction between the wrap and NSM bars as the stiffness of the NSM-wrapped specimens was changed even before NSM specimens reached their peak load. The effect is more pronounced for specimens with more NSM bars. It means the bars of NSM specimens started to buckle before their specimens' peak load. On the other hand, the FRP wrap controlled the buckling of the NSM bars and kept the bars straight contributing to the axial stiffness of the specimens. The little drops in NSM-wrapped specimens' curve near peak load indicate the crushing of at least one NSM bar, which was compatible with noises heard during the tests. Even after crushing of one NSM bar, the specimens kept resisting until more bars crushed, and finally the FRP wrap was ruptured in the hoop direction.

Based on the data presented in Table 2, the specimens with 4, 6, and 8 NSM bars wrapped with BFRPs peaked at higher axial loads with the average gain of 47.2, 58.2, and 43.3% with respect to the NSM specimens without wraps, respectively. The FRP wrap was more effective on specimens with 6 NSM bars than 8 NSM bars. This indicates that over-reinforcing the concrete specimens with longitudinal NSM bars decreased the integrity of the concrete, which weakened the lateral support of concrete for the NSM bars making them more vulnerable to axial crushing.

As presented in Figure 8 and the data presented in Table 2, the axial strain of the specimens with 4, 6, and 8 NSM bars wrapped with BFRPs at peak load showed the average gain of 395.2, 148.6, 49.2%, respectively, with respect to that of the NSM specimens without wrapping. Moreover, the lateral strain of the specimens with 4, 6, and 8 NSM bars wrapped with BFRPs at peak load showed the average gain of 580.6, 448.3, 195.5%, respectively, with respect to that of the specimens without wrapping. It means the effect of BFRP wraps on the axial and lateral deformability of the NSM specimens decreased by increasing number of NSM bars as it is shown in Figure 8. Overall, the NSM-wrap system of longitudinal NSM GFRP bars and lateral BFRP wrapping was effective on upgrading the performance of the concrete specimens. A moderate level of longitudinal NSM GFRP bars reinforcement ratio (4.3% in this study) seems more effective than low (2.9%) and high (5.7%) reinforcement ratios of NSM bars.

3.4. Contribution of NSM GFRP Bars

Extending the contribution of longitudinal NSM bars in load carrying of concrete specimens through the lateral support of the wrap was the main motivation of this study. Figure 9 shows the variation of NSM bars contribution with respect to the axial stain of the specimens. The contribution is expressed in the percentage of total load supported by the NSM bars. Per Figure 2, the stress-strain behavior of the GFRP bars in compression is elastic linear. Thus, the stress of

NSM bars was obtained by multiplying the axial strain of the bars (i.e. average of two strain gauges on the bars) by elastic modulus of the bars in compression (i.e. 45.5 GPa). Then, the total load carried by the NSM bars in each specimen was calculated based on total cross-sectional area of the bars time the stress. Finally, the NSM bars contribution at a given strain was obtained by dividing the total NSM bars load over the total load of the specimen and presented in percentage.

As shown in Figure 9, the NSM bars contribution started from a range between 6 to 12% (depending on NSM reinforcement ratio) and increased as the axial strain increased with an almost linear trend. Per Table 2, when specimens with 4, 6, and 8 NSM bars (i.e. without wrapping) reached their peak load, the NSM bars contribution reached to the average of 11.4, 17.4, and 23.6%, respectively. The average strain of NSM specimens at peak load is shown with a vertical line in Figure 9. It clearly shows that after this line the NSM bars contribution increased with a rapid rate and deviated from the linear trend. This is due to softening branch of load-strain behaviors and the fact that concrete contribution decreased until either the specimens lost the integrity or the test was terminated.

As shown in Figure 9, the NSM bars contribution of specimens wrapped with BFRPs is completely different that those without the wrap. The figure indicates that the contribution increased as the axial strain increased with an almost linear trend until the BFRP wrap ruptured in the hoop direction. Per Table 2, when NSM-wrapped specimens with 4, 6, and 8 bars reached their peak load, the NSM bars contribution reached to the average of 19.3, 30.6, and 33.4%, respectively. Overall, the wrapping system effectively prevented the premature failures of the NSM bars and extended the contribution of the bars from an average of 17.5% in the NSM specimens to an average of 27.7% in the NSM-wrap specimens.

Figure 10 compares the NSM bars contribution at peak load of all specimens. It clearly shows that the wrapping increases the contribution of NSM bars significantly. The contribution of NSM bars in the specimens with 4, 6, and 8 bars wrapped with two layers of BFRPs increased 69.0, 75.3, and 41.7%, respectively, with respect to the specimens without the wrapping. The highest increase was observed in specimens with 6 NSM bars.

Based on the results of the coupon tests presented in Figure 2, the crushing strain of GFRP bars is also presented with a vertical line at the strain of 0.0122 mm/mm in Figure 9. It clearly indicated that the NSM bars in the specimens without wrapping experienced about one third of the bars' crushing strain at the peak load and they never experience more than half of the crushing strain after the peak load. The figure also indicates that the wrapping extended the strain of NSM bars to an average 83% of the crushing strain of the bars. It shows the effectiveness of the NSM-wrap system to prevent local buckling of the NSM bars and extend their contribution to a strain level close to the crushing point of the bars.

3.5. Rupture Strain of BFRP Wraps

Figure 11 compares the lateral (hoop) strain of NSM-wrapped specimens at peak load with the tensile rupture strain of BFRP flat coupons. It indicates that the strain decreased as the number of NSM bars increased. However, the strain never reached the tensile rupture strain of BFRP flat coupons. The premature failure is known as the strain efficiency of FRP wraps (Chen et al. 2011; Pessiki et al. 2001; Sadeghian Fam 2014). To quantify the premature rupture of BFRP wraps with respect to flat coupon test result, the strain efficiency factor (κ_ε) of each specimen was calculated as follows:

$$\kappa_\varepsilon = \frac{\varepsilon_{h,rup}}{\varepsilon_{fu}} \quad (1)$$

where $\varepsilon_{h,rup}$ is the hoop strain in the wrap at failure and ε_{fu} is the flat coupon's rupture strain in tension. Using the equation, the strain efficiency factor of each specimens was calculated. The strain efficiency factor of NSM-wrapped specimens with 4, 6, and 8 bars was obtained 0.89, 0.85, and 0.41, respectively. The average strain efficiency factor of all NSM-wrapped specimens was 0.72, which is compatible with the average of 0.67 obtained by Sadeghian and Fam (2014) based on 454 cylinders wrapped with unidirectional FRPs. It means the premature rupture of BFRP wraps of NSM-wrapped specimens of this study is not much different than the premature ruptures of specimens wrapped only with FRPs (without NSM bars).

It should be noted that the strain efficiency factor of FRP wrap is not a constant factor. Multiple theories (Sadeghian and Fam 2014; Chen et al. 2012; Smith et al. 2010; Lignola et al. 2012; Vincent and Ozbakkaloglu 2016; Wu and Jiang 2013; Sadeghian et al. 2018) have been proposed on influential parameters including the multi-axial state of stress in FRP wrap, geometrical discontinuity due to FRP overlap and concrete cracking, FRP wrap curvature, and geometrical imperfections, however there is no mechanics-based theory to consider synergy of all parameters. As a result, ACI 440.2R-17 (2007) implemented a constant strain efficiency factor as presented in Eq. (1). This study also adopts the concept of a constant factor until a synergic theory is developed.

Overall, the NSM-wrap method of strengthening presented in this study was effective extending the contribution of NSM bars without changing the mode of failure of the wrap in comparison with traditional wrapping method. It should be noted that the results obtained from this study and effectiveness of the NSM-wrap system based on the small cylinder tests can't directly be extended to full-scale columns, due to size, support, absence of internal steel bars and

other differences. The NSM-wrap system needs to be applied to large-scale concrete columns with internal steel bars under pure axial and combined axial-bending loadings for further verifications.

4. ANALYTICAL STUDY

In this section, an analytical study is presented to study the effect of the proposed NSM-wrapped NSM-wrap system on the performance of reinforced concrete columns under pure axial load and combined axial load and bending moment.

4.1. Effect of NSM-Wrap System on Axial Capacity

The NSM-wrap system can enhance the axial capacity P_u of the test cylinder via both longitudinal NSM FRP bars and the confinement due to the transverse FRP wraps as follows:

$$P_u = P_c + P_f \tag{2}$$

where P_c is the contribution of confined concrete and P_f is the contribution of longitudinal NSM FRP. The contribution of confined concrete can be obtained based on the confinement model of ACI 440.2R-17 (2007) as follows:

$$P_c = f'_{cc}\left(A_g - A_f\right) \tag{3}$$

where f'_{cc} is the compressive strength of confined concrete, A_g is the gross cross-sectional area, and A_f is the total area of longitudinal NSM FRP bars. In the confinement model, which was initially adopted from Lam and Teng (2003), both the compressive strength f'_{cc} and ultimate strain ε_{ccu} of confined are a function of the effective hoop strain of FRP wrap. In this analytical study, the effective hoop strain and all required factors (e.g. κ_ε=0.55) and equations were directly adopted from ACI 440.2R-17 (2017).

The contribution of longitudinal NSM FRP bars can be calculated based on the linear-elastic behavior of FRP bars at the ultimate strain ε_{ccu} of confined concrete as follows:

$$P_f = E_{fc}\varepsilon_{ccu}A_f \quad (4)$$

where E_{fc} is the elastic modulus of FRP bars in compression. This analysis can be also performed at any given level of axial strain to compute corresponding contribution of confined concrete and longitudinal NSM bars. The stress-strain behavior of confined concrete is also adopted from ACI 440.2R-17 (2017) and the stress-strain behavior of FRP bars is considered as linear-elastic as observed by Fillmore and Sadeghian (2018).

The model was applied for the cylinders with NSM-wrap system tested in this study (i.e., NSM-4-W, NSM-6-W, and NSM-8-W) and the predicted load-strain behavior are plotted along with the experimental curves in Fig. 12. For a better understanding of the effect of the NSM-wrap system on axial behavior of the cylinders, the behavior of cylinders strengthened only with wrapping is also predicted. At the maximum useable axial strain, the results indicate a gain of 21, 32, and 43% for NSM-4-W, NSM-6-W, and NSM-8-W with respect to the case of using only wrapping system, respectively. It should be highlighted that by increasing the number of longitudinal NSM bars of the NSM-wrap system, the FRP wrap experienced a rupture at lower strain. For NSM-8-W with 8 NSM FRP bars, the strain corresponding to the peak load is about 60% of the maximum useable axial strain of 0.01 mm/mm per ACI 440.2R-17 (2017). This premature failure at a high longitudinal reinforcement ratio of 5.7% might be due to excessive number of NSM grooves and negative effect of them on the integrity of the concrete causing too many sharp corners punching the FRP wrap. Until further research on large-scale specimens, a lighter amount of longitudinal NSM FRP seems more appropriate for the NSM-wrap system.

4.2. Effect of NSM-Wrap System on Interaction Diagram

In this section, the effect of the NSM-wrap system on the axial load – bending moment interaction diagram of plain and reinforced concrete columns is investigated. An analytical model was

developed based on the cross-sectional analysis of a circular concrete section with and without steel rebar. It assumes linear strain profile and perfect bond between concrete, steel, NSM FRP, and FRP wrap. The behavior of FRP bars and wraps are summed linear elastic. The behavior of steel rebars is considered elastic-perfect plastic. The behavior of concrete under pure axial compression is based on the confinement model of ACI 440.2R-17 (2017) and the effect of load eccentricity is considered based on the variable confinement model proposed by Fam et al. (2003). The variable confinement model assumes the full confinement at the pure axial compression gradually reduces to zero confinement at the extreme pure bending condition. The ultimate compressive strain of unconfined concrete is assumed 0.003 mm/mm. Tensile strength of concrete is neglected.

The interaction diagram model takes the geometrical and materials properties of a circular RC section strengthened with NSM-wrap system and generates stress-strain curve of confined concrete as explained earlier. Then at any given eccentricity, it generates the reduced confined stress-strain curve due to the eccentricity according to the procedure proposed by Fam et al. (2003). Then, by assuming a neutral axis depth and reaching concrete strain at the extreme compressive layer to the corresponding ultimate strain of confined concrete at the given eccentricity, the internal forces and moments of confined concrete, steel rebars, and longitudinal FRPs are computed. The location of neutral axis is changed until the equilibrium of internal and external forces and moments are satisfied. The strain in compressive and tensile longitudinal FRPs are also calculated to ensure they do not reach to their corresponding failure strains. If that was the case, the strain profile would be adjusted to the failure mode and all calculated would be repeated until equilibrium equations were satisfied. The final location of neutral axis under the given eccentricity provides the axial load and bending moment capacity of the cross-section. By changing the eccentricity,

corresponding axial load and bending moment are calculated until the full interaction diagram is formed.

As there is no test data available in the literature on NSM-wrapped circular RC columns (at this time), the model was applied to a set of test data on the effects of slenderness by Fitzwilliam and Bisby (2010) on circular RC columns wrapped with carbon FRP (CFRP) fabrics. They tested 18 columns with a diameter of 152 mm and variable lengths (300, 600, and 1200 mm) under eccentric loading, however three of the columns were wrapped with multiple layer of CFRP with layers in both hoop and longitudinal directions. The test results of the three columns are presented in Table 3. For example, columns 1200C-1-4-A was 1200 mm long, wrapped with one layer of hoop CFRP and four layers of longitudinal CFRP. The actual eccentricity of each specimen at mid-height under peak load along with the peak load and corresponding moment at the peak load are presented in the table. The model presented in the current study was applied to the test specimens and the peak load and corresponding moment were calculated and presented in Table 3 along with the test-to-model ratios. The test-to-model ratios are 1.02, 1.09, and 1.12 with an average of 1.08, which shows a good agreement between the model and test results. The model slightly under-predicts the failure loads, which is at the safe side.

The model was also applied to the geometry of the cylinders tested in this study and the results are presented in Fig. 13(a). As shown, the interaction diagrams of the NSM-wrap cylinders are enlarged by increasing the number of NSM FRP bars. Also, the interaction diagrams of the NSM-wrap cylinders are significantly larger than that of the wrapped cylinder, specially under high eccentricities.

To have a better understanding of the effect of the NSM-wrap system on interaction diagrams, the model was applied to a steel reinforced concrete (RC) section with a diameter of 250

mm. The section is reinforced with six steel rebar providing the reinforcement ratio of about 2%, which is a low to moderate reinforcement ratio. Then the section was strengthened with an NSM-wrap system of six NSM FRP bars with the same cross-sectional area of steel bars and minimum FRP wrapping per ACI 440.2R-17(2017). Fig. 13(b) shows the cross-section and the interaction diagrams generated using the model. The results indicate that the conventional wrapping system is effective under low eccentricities, however it is not effective under high eccentricities. On the other hand, the proposed NSM-wrap system is effective for all range of eccentricities. For example, the NSM-wrap system increased the capacity of control RC section under pure axial and pure bending loading about 47 and 65%, respectively.

It should be noted that the effectiveness of the NSM-wrap system under combined axial load and bending moment needs to be investigated experimentally to verify the preliminary results of this study. Because the current study involves the use of small-scale specimens and size effect is an important matter to study, the NSM-wrap system should be applied to large-scale specimens to study before considering for any applications.

5. CONCLUSIONS

Strengthening existing concrete columns using FRPs in the form of longitudinal NSM bars has not gained much attention due to the possibility of premature crushing and/or buckling of NSM bars. In this paper, a total of 21 cylindrical concrete specimens were used to study the behavior of a NSM-wrap system of NSM GFRP bars and BFRP wrapping system. The specimens were instrumented with strain and displacement gauges and loaded under uniaxial compression until failure. An analytical model was also developed to predict the load-strain behavior of the NSM-wrap test specimens. The model was further expanded to evaluate the performance of the NSM-

wrap system under combined axial load and bending moment loadings. The following conclusions can be drawn from the study:

- In concrete specimens with NSM bars, the bars did not show any signs of crushing until the concrete bulged and cracked significantly. The crushing was combined with local buckling of the bars.
- The BFRP wrap changed the behavior of the NSM specimens significantly, increasing both peak load and its corresponding strain. A moderate level of longitudinal NSM GFRP bars reinforcement ratio (4.3% in this study) was more effective than low (2.9%) and high (5.7%) reinforcement ratios of NSM bars.
- The combination of longitudinal NSM GFRP bars and lateral BFRP wrapping was effective on upgrading the performance of concrete specimens. The wrapping system effectively extended the contribution of the bars from an average of 17.5% in the NSM specimens to an average of 27.7% in the NSM-wrap specimens.
- The strain efficiency factor of NSM-wrapped specimens with 4, 6, and 8 bars was obtained 0.89, 0.85, and 0.41, respectively. The average strain efficiency factor of all NSM-wrapped specimens was 0.72, which is compatible with the average of 0.67 obtained from the literature.
- The analytical model showed that the NSM-wrap system can be effective for both low and high eccentricities. As the results were based on small-scale specimens, in order to consider the size effect, more research is needed on the behavior of large-scale concrete columns with internal steel bars strengthened with the NSM-wrap system under pure axial and combined axial-bending loadings.

6. ACKNOWLEDGEMENTS

The authors would like to acknowledge the financial support of NSERC and Dalhousie University. Randy Nason of Pinnacle Agencies Ltd (Dartmouth, NS, Canada) is thanked for providing the BASF adhesive.

7. REFERENCES

ACI 440.1R-15. 2015. Guide for the Design and Construction of Structural Concrete Reinforced with Fiber-Reinforced Polymer (FRP) Bars, American Concrete Institute, Farmington Hills, Michigan, USA.

ACI 440.2R-17. 2017. Guide for the Design and Construction of Externally Bonded FRP Systems for Strengthening Concrete Structures, American Concrete Institute, Farmington Hills, Michigan, USA.

Aslan FRP. 2018. Aslan 100™ glass fiber reinforced polymer (GFRP) rebar for infrastructure solutions. Owens Corning Infrastructure Solutions, Seward, NE, USA.

ASTM D3039. 2008. Standard Test Method for Tensile Properties of Polymer Matrix Composite Materials, American Society for Testing and Materials, West Conshohocken, PA, USA.

ASTM D7205. 2006. Standard Test Method for Tensile Properties of Fiber Reinforced Polymer Matrix Composite Bars, American Society of Testing and Materials, West Conshohocken, PA, USA.

BASF. 2014. MasterEmaco® ADH 1420 General-purpose gel epoxy adhesive. BASF Corporation, Shakopee, MN, USA.

Bisby, L., and Ranger, M. 2010. Axial–flexural interaction in circular FRP-confined reinforced concrete columns. Construction and Building Materials, 24(9), 1672-1681.

Bournas, D. A., and Triantafillou, T. C. 2009. Flexural strengthening of reinforced concrete columns with near-surface-mounted FRP or stainless steel. ACI Structural Journal, 106(4), 495.

Chen, J. F., Li, S. Q., and Bisby, L. A. 2012. Factors affecting the ultimate condition of FRP-wrapped concrete columns. Journal of Composites for Construction, 17(1), 67-78.

Chen, J. F., Li, S. Q., Bisby, L. A., and Ai, J. 2011. FRP rupture strains in the split-disk test. Composites Part B: Engineering, 42(4), 962-972.

De Lorenzis, L., and Nanni, A. 2001. Characterization of FRP rods as near-surface mounted reinforcement. Journal of Composites for Construction, 5(2), 114-121.

El-Maaddawy, T., and El-Dieb, A. S. 2010. Near-surface-mounted composite system for repair and strengthening of reinforced concrete columns subjected to axial load and biaxial bending. Journal of composites for construction, 15(4), 602-614.

Fam, A., Flisak, B., and Rizkalla, S. 2003. Experimental and analytical modeling of concrete-filled FRP tubes subjected to combined bending and axial loads. ACI Struct. J, 100(4), 499-509.

Fillmore, B., and Sadeghian, P. 2018. Contribution of Longitudinal GFRP Bars in Concrete Cylinders under Axial Compression. Canadian Journal of Civil Engineering. 45 (6), 458-468.

Fiore, V., Scalici, T., Di Bella, G., and Valenza, A. 2015. A review on basalt fibre and its composites. Composites Part B: Engineering, 74, 74-94.

Fitzwilliam, J., and Bisby, L. A. 2010. Slenderness effects on circular CFRP confined reinforced concrete columns. Journal of Composites for Construction, 14(3), 280-288.

Hadhood, A., Mohamed, H. M., Ghrib, F., and Benmokrane, B. 2017. Efficiency of glass-fiber reinforced-polymer (GFRP) discrete hoops and bars in concrete columns under combined axial and flexural loads. Composites Part B: Engineering, 114, 223-236.

Hassan, T., and Rizkalla, S. 2003. Investigation of bond in concrete structures strengthened with near surface mounted carbon fiber reinforced polymer strips. Journal of Composites for Construction, 7(3), 248-257.

Hosseini, M. M., Dias, S. J., and Barros, J. A. 2014. Effectiveness of prestressed NSM CFRP laminates for the flexural strengthening of RC slabs. Composite Structures, 111, 249-258.

Karim, H., Sheikh, M. N., and Hadi, M. N. 2016. Axial load-axial deformation behaviour of circular concrete columns reinforced with GFRP bars and helices. Construction and Building Materials, 112, 1147-1157.

Khorramian, K. and Sadeghian, P. 2019. Material Characterization of GFRP Bars in Compression Using a New Test Method. ASTM Journal of Testing and Evaluation, 49(2), In press: https://doi.org/10.1520/JTE20180873.

Khorramian, K., and Sadeghian, P. 2017. Experimental and analytical behavior of short concrete columns reinforced with GFRP bars under eccentric loading. Engineering Structures, 151, 761-773.

Lam, L., and Teng, J. G. 2003. Design-oriented stress–strain model for FRP-confined concrete. Construction and building materials, 17(6-7), 471-489.

Lignola, G. P., Nardone, F., Prota, A., and Manfredi, G. 2012. Analytical model for the effective strain in FRP-wrapped circular RC columns. Composites Part B: Engineering, 43(8), 3208-3218.

Pessiki, S., Harries, K. A., Kestner, J., Sause, R., and Ricles, J. M. 2001. The axial behavior of concrete confined with fiber reinforced composite jackets. J. Compos. Constr, 5(4), 237-245.

Rocca, S., Galati, N., and Nanni, A. 2009. Interaction diagram methodology for design of FRP-confined reinforced concrete columns. Construction and Building Materials, 23(4), 1508-1520.

Sadeghian, P., and Fam, A. 2014. A rational approach toward strain efficiency factor of fiber-reinforced polymer-wrapped concrete columns. ACI Structural Journal, 111(1), 135.

Sadeghian, P., and Fam, A. 2014. Strengthening slender reinforced concrete columns using high-modulus bonded longitudinal reinforcement for buckling control. Journal of Structural Engineering, 141(4), 04014127.

Sadeghian, P., Seracino, R., Das, B., and Lucier, G. 2018. Influence of geometry and fiber properties on rupture strain of cylindrical FRP jackets under internal ICE pressure. Composite Structures, 192, 173-183.

Smith, S. T., Kim, S. J., and Zhang, H. 2010. Behavior and effectiveness of FRP wrap in the confinement of large concrete cylinders. Journal of Composites for Construction, 14(5), 573-582.

Tobbi, H., Farghaly, A. S., and Benmokrane, B. 2012. Concrete columns reinforced longitudinally and transversally with glass fiber-reinforced polymer bars. ACI Structural Journal, 109(4), 551.

Unistar 2016. Basalt Unidirectional Fabric B-T300. Universal Star Group Limited, Ningbo, China.

Vincent, T., and Ozbakkaloglu, T. 2016. Influence of overlap configuration on compressive behavior of CFRP-confined normal-and high-strength concrete. Materials and Structures, 49(4), 1245-1268.

West System. 2015. West System 105 Epoxy Resin® and 206 Slow Hardener®. Gougeon Brothers, Inc., Bay City, MI, USA.

Wu, Y. F., and Jiang, J. F. 2013. Effective strain of FRP for confined circular concrete columns. Composite Structures, 95, 479-491.

Table 1. Test matrix.

Group #	Specimen ID	Number of identical specimens	Number of NSM bars	Number of FRP wrap layers
1	**Plain**	3	0	0
2	**NSM-4**	3	4	0
3	**NSM-6**	3	6	0
4	**NSM-8**	3	8	0
5	**NSM-4-W**	3	4	2
6	**NSM-6-W**	3	6	2
7	**NSM-8-W**	3	8	2
	Total	21	-	-

Table 2. Summary of test results.

Specimen ID	Peak load (kN)		Axial strain at peak load (mm/mm)		Lateral strain at peak load (mm/mm)		NSM bars force at peak load (kN)		NSM bars contribution at peak load (%)	
	AVG	SD	AVG	SD	AVG	SD	AVG	SD	AVG	SD
Plain	707	14	0.0030	0.0002	0.0020	0.0003	-	-	-	-
NSM-4	729	22	0.0034	0.0002	0.0033	0.0006	83	10	11.4	1.2
NSM-6	722	21	0.0033	0.0003	0.0039	0.0003	126	4	17.4	0.2
NSM-8	765	12	0.0037	0.0002	0.0036	0.0002	180	3	23.6	0.2
NSM-4-W	1072	88	0.0167	0.0027	0.0224	0.0048	207	77	19.3	6.6
NSM-6-W	1142	53	0.0083	0.0040	0.0216	0.0039	347	43	30.6	5.2
NSM-8-W	1096	46	0.0055	0.0004	0.0105	0.0024	367	47	33.4	2.8

Table 3. Performance of the interaction diagram model against the test data by Fitzwilliam and Bisby (2010).

Specimen ID	Eccentricity at mid-height (mm)	Test		Model		Test to model ratio
		Peak load (kN)	Moment at peak (kN-m)	Peak load (kN)	Moment at peak (kN-m)	
300C-1-2-A	20.6	681	14.03	622	12.82	1.09
1200C-1-2-A	30.3	582	12.63	521	15.78	1.12
1200C-1-4-A	29.4	671	19.72	659	19.39	1.02
Average						**1.08**

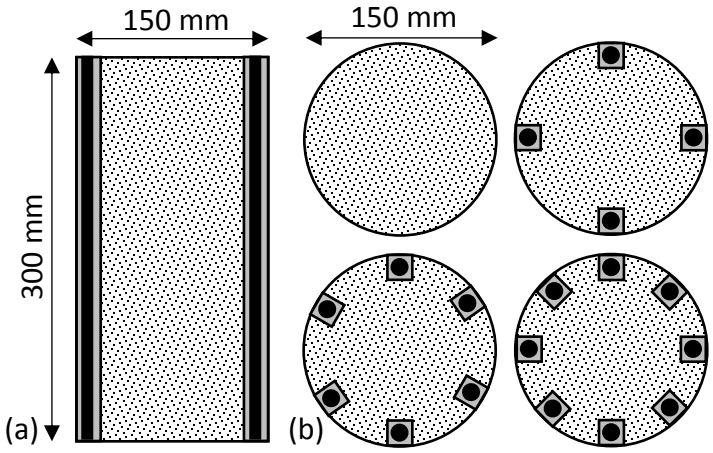

Figure 1. Geometry of NSM specimens: (a) elevation view; (b) cross-section of plain and NSM-4, -6, and -8 bar specimens.

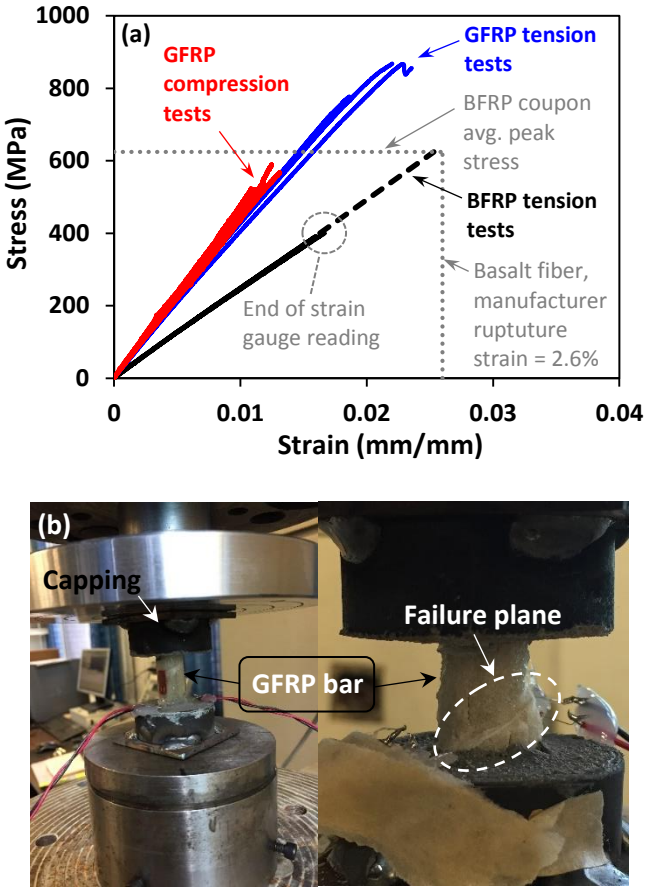

Figure 2. FRP material properties: (a) stress-strain behavior in tension and compression; and (b) GFRP bar compression test.

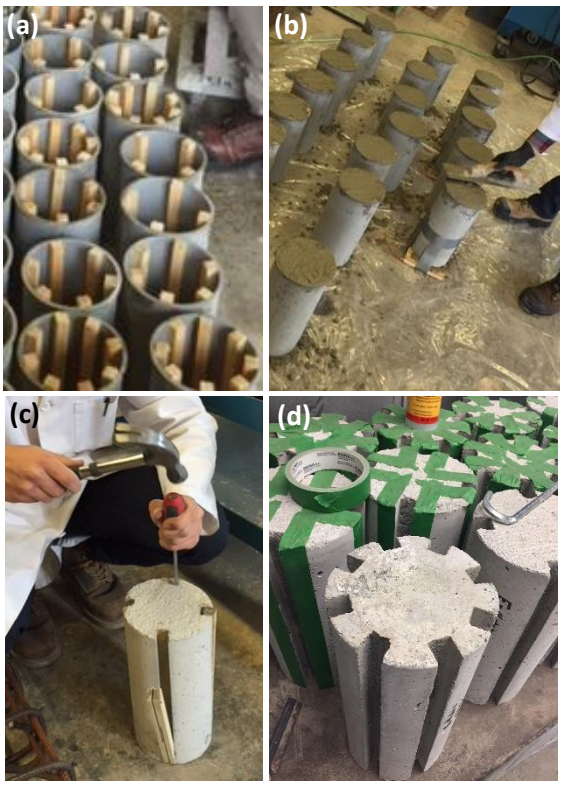

Figure 3. Specimen fabrication: (a) formwork with temporary wooden sticks installed for NSM grooves; (b) concrete placed; (c) removing of wooden sticks after concrete curing; and (d) grooved ready for NSM bars.

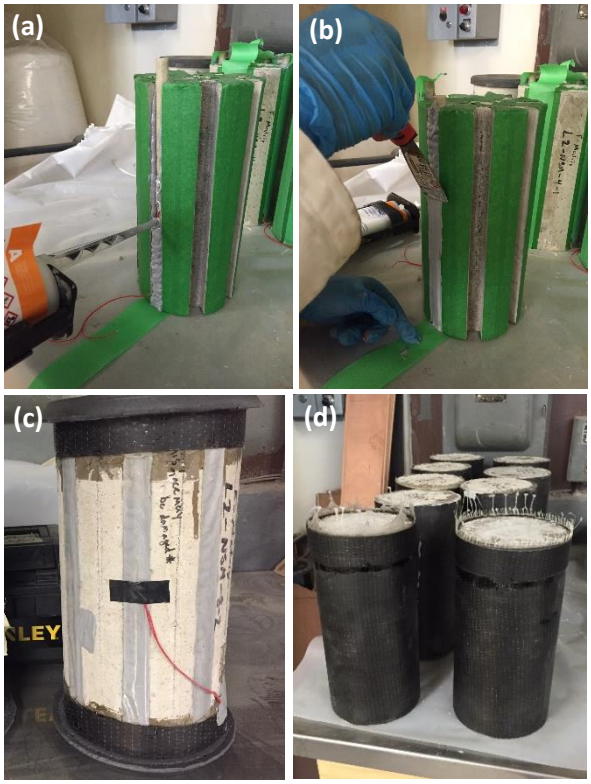

Figure 4. NSM-wrap strengthening procedure of concrete cylinders: (a) NSM bar inserted in groove; (b) groove surface preparation; (c) NSM specimen; (d) NSM-wrapped specimens.

Figure 5. Instrumentation and test setup: (a) GFRP bars strain gauged; (b) LVDT arrangement of NSM specimens; (c) LVDT arrangement and test setup of NSM-wrapped specimens; and (d) schematic instrumentation of NSM-wrapped specimens.

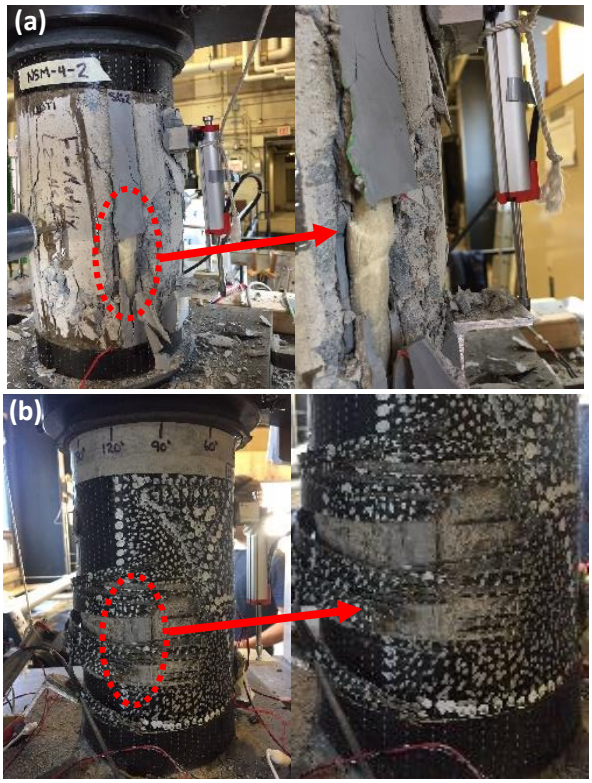

Figure 6. Failure modes: (a) NSM specimen and (b) NSM-wrapped specimens.

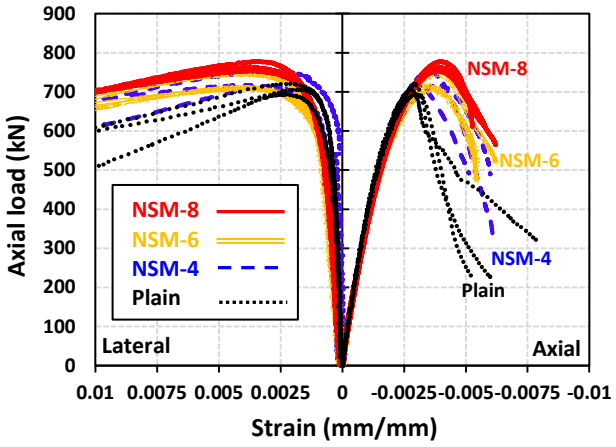

Figure 7. Load-strain behavior of plain and NSM specimens.

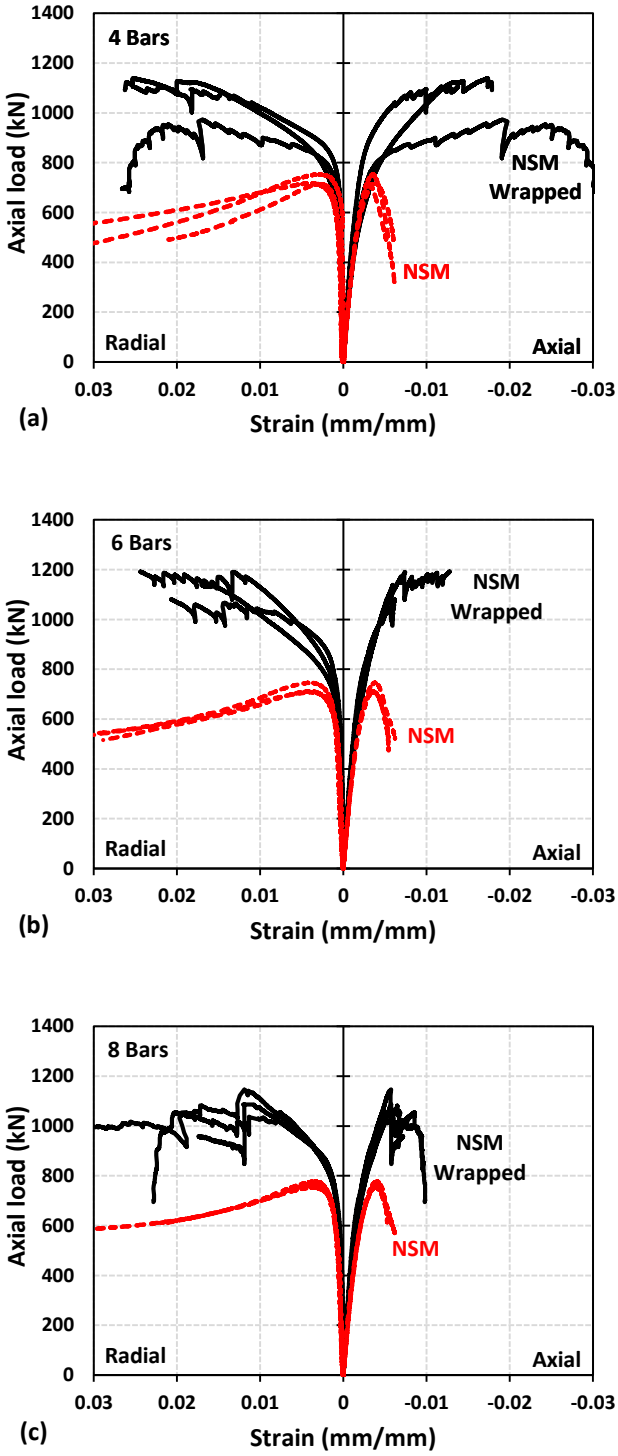

Figure 8. Load-strain behavior of specimens with (a) 4, (b) 6, and (c) 8 NSM GFRP bars with and without BFRP wrapping.

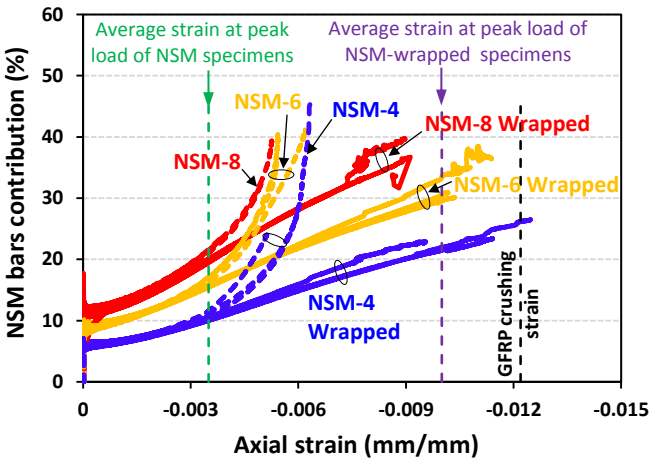

Figure 9. Effect of transverse wrapping on contribution of longitudinal NSM bars in the axial load bearing capacity of test specimens.

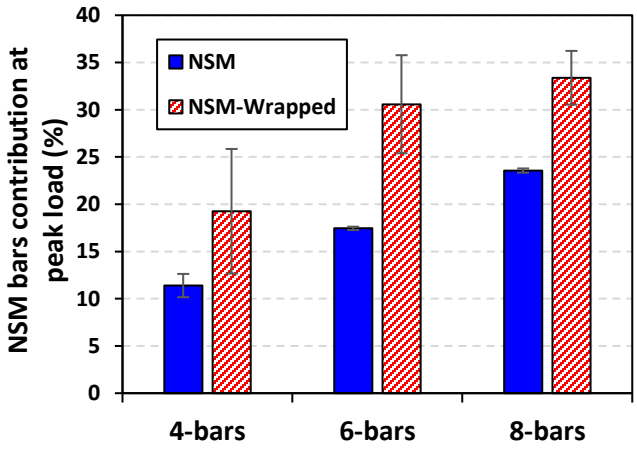

Figure 10. NSM bars contribution at peak load with and without wrapping.

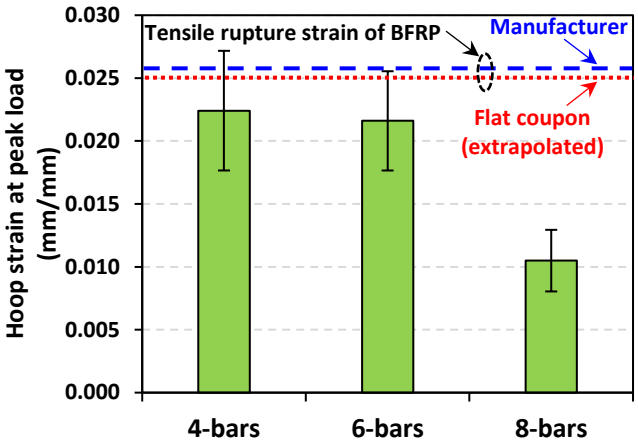

Figure 11. Lateral (hoop) strain of NSM-wrapped specimens.

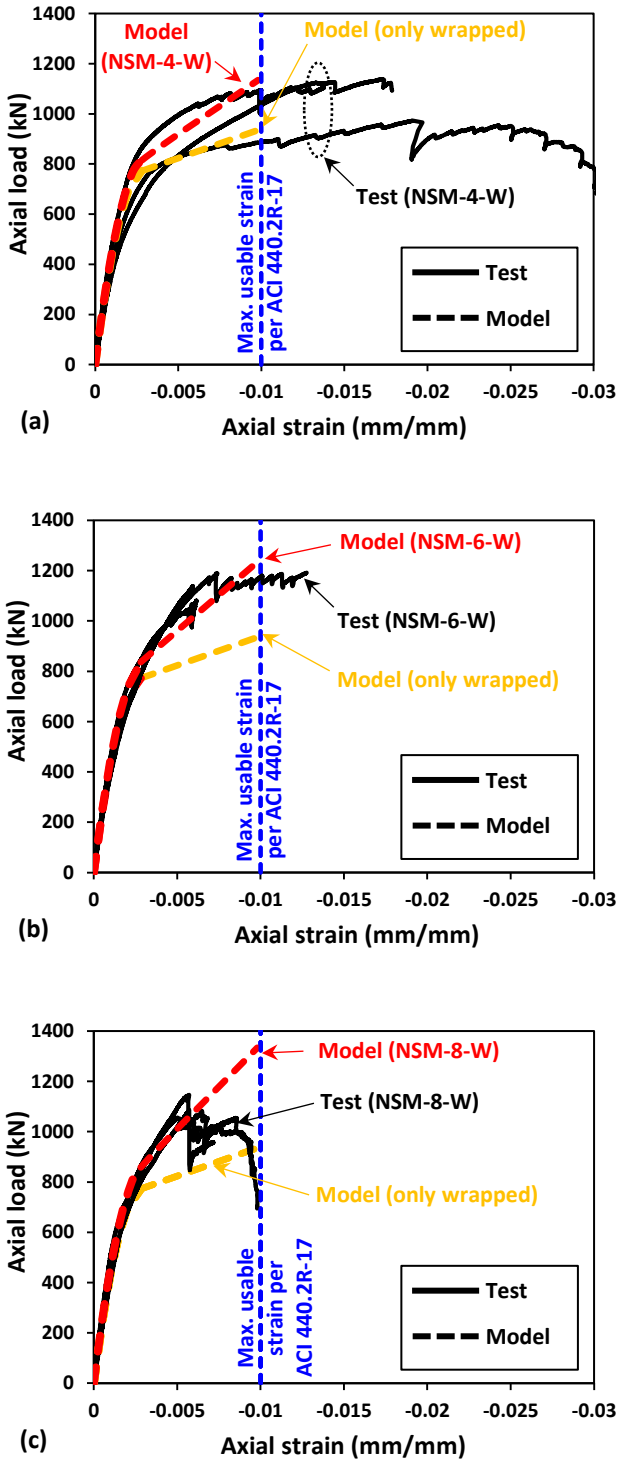

Figure 12. Comparison of the experimental results and analytical model developed based on ACI 440.2R-17 for FRP-wrapped concrete cylinders with and without NSM bars.

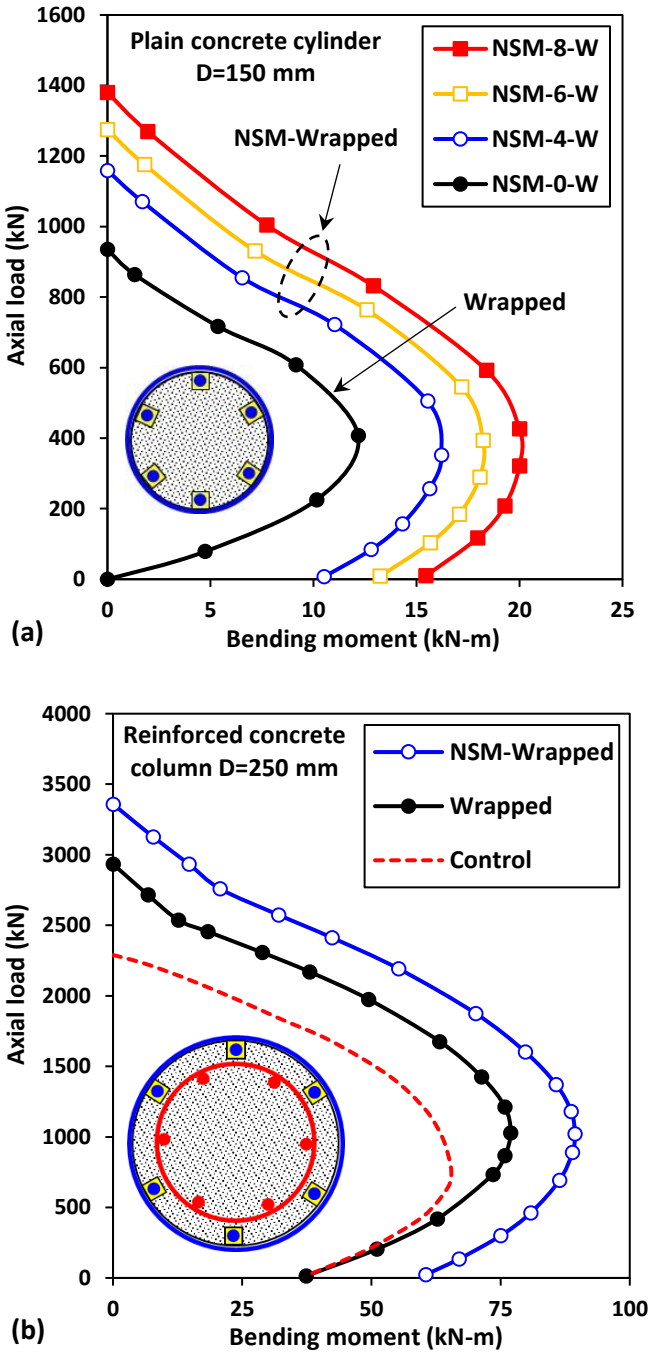

Figure 13. Comparison of axial load – bending moment interaction diagrams of proposed NSM-wrap and conventional wrapping systems: (a) the tested plain concrete cylinders (D=150 mm); and a reinforced concrete column (D=250 mm).